Available online at www.sciencedirect.com
ScienceDirect
Trans. Nonferrous Met. Soc. China 29(2019) 1549−1559
Transactions of Nonferrous Metals Society of China
www.tnmsc.cn

Effect of B_2O_3 addition on oxidation induration and reduction swelling behavior of chromium-bearing vanadium titanomagnetite pellets with simulated coke oven gas

Wei-dong TANG[1], Song-tao YANG[2], Xiang-xin XUE[1]

1. School of Metallurgy, Northeastern University, Shenyang 110819, China;
2. School of Materials and Metallurgy, University of Science and Technology Liaoning, Anshan 114051, China

Received 6 October 2018; accepted 28 February 2019

Abstract: The oxidation induration and reduction swelling behavior of the chromium-bearing vanadium titanomagnetite pellets (CVTP) with B_2O_3 addition were investigated. Besides, the reduction swelling index (RSI) and compressive strength (CS) of the reduced CVTP were also examined using the simulated coke oven gas (COG). The results suggested that the CS of CVTP was increased from 2448 to 3819.2 N, while the porosity of CVTP was decreased from 14.86% to 10.03% with the increase in B_2O_3 addition amounts. Moreover, the B_2O_3 mainly existed in the forms of $TiB_{0.024}O_2$ and Fe_3BO_5 in both CVTP and the reduced CVTP. Specifically, the CS of the reduced CVTP was elevated from 901 to 956.2 N, while the RSI was reduced from 5.87% to 3.81% as the B_2O_3 addition amounts were increased. Taken together, B_2O_3 addition would facilitate the aggregation and diffusion of metallic iron particles, which contributed to reducing the formation of metal iron whiskers and weakening the reduction swelling behavior.

Key words: B_2O_3; oxidation induration; reduction swelling index; coke oven gas; chromium-bearing vanadium titanomagnetite pellets

1 Introduction

The blast furnace (BF) has been extensively employed during the ironmaking process, which has become the primary ironmaking method. Nevertheless, the massive utilization of coke and coal in BF will give rise to the generation of plenty of carbon monoxide (CO) and carbon dioxide (CO_2). Noteworthily, CO_2 emission from the iron and steel industry accounts for about 15% of the total CO_2 emissions in China. Currently, the idle coke oven gas (COG) has exceeded 6.5×10^7 m^3 every year in the iron and steel industry. Moreover, the average heating value of COG is 18500 kJ/m^3, which is thereby a valuable fuel that can be utilized to decrease the usage of coal and coke in BF. Besides, the COG has contained 60.7% H_2, and COG injection has been recognized as one of the viable methods to decrease CO_2 emission and to achieve low-carbon ironmaking in BF.

The chromium-bearing vanadium titanomagnetite (CVTM) in the Panzhihua area of Sichuan Province, China, is a kind of large reserve resource, with the reserves of more than 3.5×10^9 t. CVTM is one of the largest VTM mineral resources, which is composed of Fe, Ti, V and Cr, as well as many other rare elements [1,2]. In addition, similar types of ores mainly distribute in Russia, Canada, Australia, and other places all over the world [3,4]. Many studies have been conducted on the sintering of CVTM, but few studies are available regarding the rare elements of CVTM [5,6]. On the other hand, ferroboron is usually used as the steel additive, NdFeB permanent magnet material, amorphous soft magnetic material for transformer, and raw material for cored wire. Additionally, studies on the pelletizing and reduction of B-bearing raw materials have also been carried out to further investigate ferroboron production. Furthermore, the hydrogen smelting technology using COG has also been implemented to intensify the smelting of CVTM and to reduce CO_2 emission.

MAHESWARAN et al [7] had indicated in their

Foundation item: Projects (51674084, 51174051, 51574082) supported by the National Natural Science Foundation of China
Corresponding author: Song-tao YANG, Tel: +24-83684086, E-mail: yangsongtao1984@163.com;
Xiang-xin XUE, Tel: +24-83681711, E-mail: xuexx@mail.neu.edu.cn
DOI: 10.1016/S1003-6326(19)65062-4

study that the boron could enhance the ductility of powder metallurgy steels, which could be ascribed to the generation of liquid phases. BIAN et al [8] investigated that the FeO−B_2O_3 fluxes, which served as the extraction agent, contributed to obtaining the rare earth oxides from the magnet scraps. WANG et al [9] had explored the reduction and melting separation of ludwigite pellets, as well as the properties of B-rich slag. FU et al [10] had examined the recovery of Mg from ludwigite ore through an innovative and clean technological route. Moreover, WANG et al [11] had detected the oxidation resistance of boron-modified carbon foams according to the low-cost slurry method. GAO et al [12] and REN et al [13] had investigated the influence of B_2O_3 on the Ti-bearing BF slag, and discovered that B_2O_3 could reduce the BF slag viscosity with the depolymerization of the structure. SUN et al [14] discovered that B_2O_3 acted as a typical network to form oxide, which could generate the BO_3 triangular, thereby resulting in a simple structure and the decreased viscosity. XU et al [15] considered that the B_2O_3 could form the low point compounds in the meantime of reducing the slag viscosity. Consequently, the B_2O_3 is beneficial to the smelting of burden in BF; however, the effect of B_2O_3 on CVTM pellets remains largely unknown. Hence, it is of essential significance to investigate the impact of B_2O_3 on pellets performance, reduction, and smelting of CVTM.

In this work, first, the effect of B_2O_3 addition on the phase compositions, compressive strength (CS), porosity, microstructure, and oxidation induration of CVTP would be analyzed. Furthermore, the impact of B_2O_3 addition on the swelling behavior of CVTP with simulated COG injection into BF would also be examined. Hopefully, these results would provide the theoretical and technical bases for the production of CVTP using the COG injection technology.

2 Experimental

2.1 Materials

The CVTM was derived from the Hongge (Sichuan, China). The chemical compositions of the CVTM are listed in Table 1. Figure 1 shows the XRD pattern of the CVTM. The main minerals of the CVTM were Fe_3O_4, $FeTiO_3$ and $FeCr_2O_4$. The B_2O_3 of analytical grade was purchased from Sinopharm Chemical Reagent Co. Ltd. (China).

Table 1 Chemical compositions of raw materials (wt.%)

TFe	FeO	TiO_2	V_2O_5	Cr_2O_3	
53.35	26.91	11.60	0.57	0.81	
CaO	SiO_2	MgO	Al_2O_3	P	S
0.96	4.71	3.33	2.82	0.02	0.26

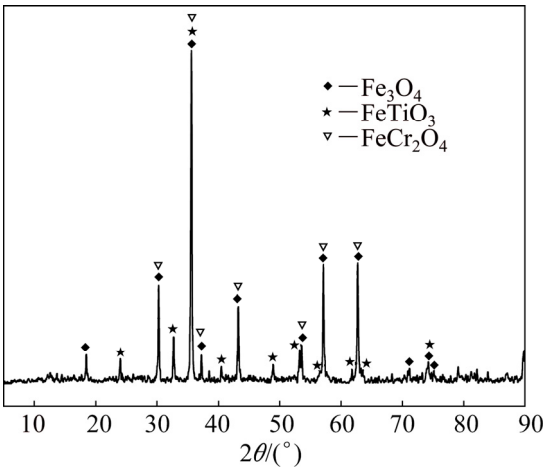

Fig. 1 XRD pattern of chromium-bearing vanadium titanomagnetite (CVTM)

2.2 Apparatus and procedure

The pelletizing process included mixing, balling, drying, oxidation induration and cooling. The main parameters of the pelletizing process included 8.0% moisture of the mixed materials, 30 min of pelletizing, green pellets with the size of 10−12 mm, drying at 105 °C for 5 h, preheating at 900 °C for 20 min, and roasting at 1200 °C for 20 min with 1.5 L/min blowing air. Subsequently, the CVTP was taken out of the muffle furnace and cooled to room temperature upon the complexion of oxidation induration.

Afterwards, the swelling behavior of the CVTP was examined using the comprehensive metallurgical measuring apparatus, as shown in Fig. 2. Firstly, the CVTP with the average size of 10−12.5 mm was placed into the constant temperature zone of the apparatus, which was then heated to the target temperature under N_2 atmosphere at the flow rate of 3 L/min. Later, moderate COG injection (150 m^3/t HM, $CO:H_2:CO_2:N_2$=40:15:10:35, vol.%) was purged into the apparatus at the flow rate of 15 L/min. Finally, the reactor was removed from the apparatus and was cooled under N_2 atmosphere upon the completion of reduction. Eventually, the reduction swelling index (RSI) and the compressive strength of the reduced CVTP (CSR) were measured. Typically, the reduction was performed at 900 °C for 60 min.

The RSI was defined as follows:

$$I_{SR}=\frac{V_t-V_0}{V_0}\times 100\% \quad (1)$$

where V_0 and V_t are the volumes of the original CVTP and the reduced CVTP, respectively (mm^3). Afterwards, the diameters of the CVTP and the reduced CVTP were measured using an electronic vernier calliper.

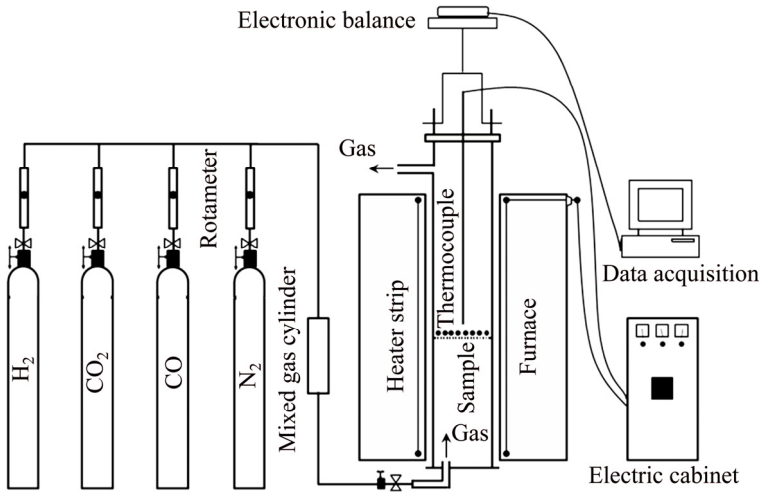

Fig. 2 Schematic diagram of experimental apparatus

2.3 Analytical methods

The chemical compositions of raw materials were tested using X-ray fluorescence (XRF, ZSXPrimus II; Rigaku, Japan). Besides, the mineral phases of both CVTM and CVTP were analyzed through X-ray diffraction (XRD, X'Pert Pro; PANalytical, Almelo, Netherlands) with Cu K_α radiation (λ=1.5406 Å) under the conditions of 40 kV and 40 mA. The scanned range was 2θ=5°−90° with a step of 0.17° and 1 s/step. Moreover, the microstructure of CVTP was detected using scanning electron microscope (SEM, Ultra Plus; Carl Zeiss GmbH, Jena, Germany) equipped with the backscattering detector (BSE) and energy disperse spectroscope (EDS). Thereafter, the CVTP was subject to thermal mounting in resin and polishing using the mirror finish for microstructure analysis. Furthermore, the porosity and pore size distribution of CVTP were tested using the mercury injection apparatus (Micromeritics Instrument Corporation, Autopore IV 9500, USA), and the compressive strength (CS) of CVTP was determined with reference to ISO4700.

3 Results and discussion

3.1 Oxidation induration of CVTP

3.1.1 Phase composition

Figure 3 shows the primary phases of CVTP under different B_2O_3 addition amounts. It could be observed that, the primary phases of CVTP without B_2O_3 addition were Fe_2O_3 and Fe_2TiO_5. When the B_2O_3 addition was increased from 2 to 6 wt.%, the peak intensities of $TiB_{0.024}O_2$ and Fe_3BO_5 would be gradually strengthened, while those of Fe_2O_3 and Fe_2TiO_5 would be weakened. Such findings indicated that the contents of $TiB_{0.024}O_2$ and Fe_3BO_5 would be increased, while those of Fe_2O_3 and Fe_2TiO_5 would be reduced. The main oxidation reactions and phase transformation of Fe_3O_4, $FeTiO_3$ and B_2O_3 in CVTP were displayed below:

$$Fe_3O_4 + O_2 \rightarrow Fe_2O_3 \quad (2)$$

$$Fe_2O_3 + FeTiO_3 + O_2 \rightarrow Fe_2TiO_5 \quad (3)$$

$$Fe_2TiO_5 + B_2O_3 \rightarrow Fe_2O_3 + TiB_{0.024}O_2 \quad (4)$$

$$Fe_3O_4 + B_2O_3 \rightarrow Fe_3BO_5 \quad (5)$$

Furthermore, the additive B_2O_3 would react with iron oxide and titanium oxide to generate $TiB_{0.024}O_2$ and Fe_3BO_5, respectively, during the oxidation process. SONMEZOGLU et al [16] suggested that the B element had a similar ionic radius to Ti, which could enter into the TiO_2 lattice to generate the B-doped TiO_2. In addition, PTAČINOVÁ et al [17] had investigated the oxidation behavior of the Fe_2O_3−B_2O_3 system, and discovered that $FeBO_3$, Fe_3BO_6, Fe_2BO_4 and Fe_3BO_5 were the intermediate products. According to the phase diagram of the B_2O_3−FeO system, the Fe_3BO_5 phase would be generated at the B_2O_3 content lower than 12 wt.%.

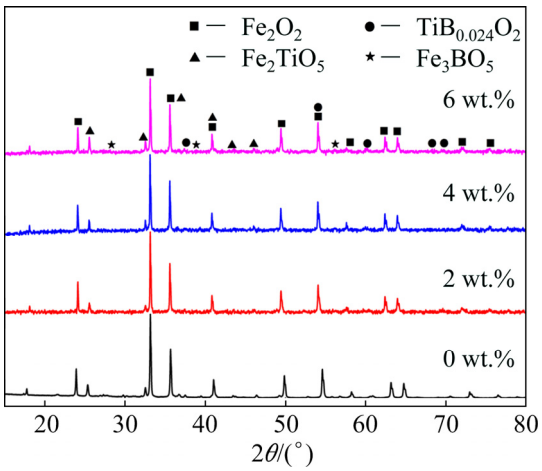

Fig. 3 XRD patterns of CVTP with different B_2O_3 addition amounts

3.1.2 Compressive strength and porosity

Figure 4 displayed the changes in CS and porosity of CVTP with different B_2O_3 addition amounts. As could be observed, CS was increased from 2448 to 3819.2 N, whereas the porosity was decreased from 14.86% to 10.03% with the increase in B_2O_3 additions. Besides, B_2O_3 addition was found to obviously increase CS, and low CS with high porosity could be obtained for CVTP in the absence of B_2O_3.

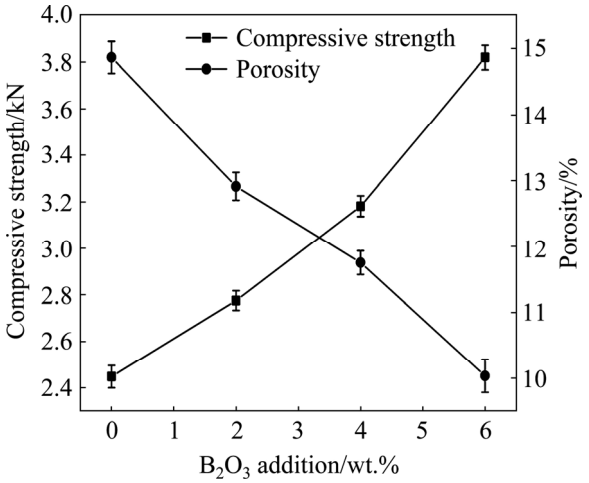

Fig. 4 Effect of B_2O_3 additions on CS and porosity of CVTP

The empirical equation between porosity and CS was displayed below [18]:

$$C = K \cdot d^{-\alpha} \cdot \exp(-\eta \cdot P) \tag{6}$$

where C indicated the CS (N), P represented the porosity of the CVTP (%), d was grain radius (cm), while K, α, and η were the coefficients.

As could be figured out from Eq. (6), CS would be decreased with the increase in porosity. OROWAN [19] had studied the equation of theoretical fracture strength of the solid material σ_{th}:

$$\sigma_{th} = \sqrt{\frac{E\gamma_s}{r_0}} \tag{7}$$

where E was indicative of the elastic modulus (GPa), γ_s was the free surface energy (J), and r_0 suggested the average distance between atoms (m).

Moreover, SPRIGGS [20] had investigated the effect of porosity on elastic modulus according to the following equation:

$$E = E_0 \exp(-\beta \cdot P_m) \tag{8}$$

where E_0 was the elastic modulus of nonporous sample, β represented an empirical constant, and P_m was the volume fraction porosity.

Hence, the relationship between theoretical fracture strength and porosity could be interpreted as

$$\sigma_{th} = \sqrt{\frac{E_0\gamma_s}{r_0 \exp(\beta \cdot P_m)}} \tag{9}$$

Based on Eq. (9), the theoretical fracture strength would be increased exponentially with the decrease in porosity, suggesting that the theoretical fracture strength would be higher in the presence of a lower porosity in pellets. Hence, the porosity would be decreased while the CS would be increased with B_2O_3 addition.

Figure 5 presents the effects of different B_2O_3 addition amounts on the pore size distribution of CVTP in the manner of histograms. It could be observed that, the pore size of CVTP mainly distributed within the range of 0−5 μm, and the proportion of micron pore size distribution of CVTP would be slightly reduced with the increase in the B_2O_3 addition amounts. Meanwhile, the proportion of large pore size distribution within the range of 5−30 μm would be reduced with the increase in the B_2O_3 addition amounts, reflecting that the incremental intrusion of mercury in micron pore size was persistently decreased. These results corresponded to the decreased porosity from 14.86% to 10.03%. It could be judged based on the increasing CS of CVTP as well as the negative correlation of CS with porosity that, the oxidation induration of CVTP would be strengthened with B_2O_3 addition. Hence, the porosity of CVTP would be reduced with the increase in B_2O_3 addition, which could be ascribed to the shrinking macropores and aggregated large-size pores.

3.1.3 Microscopic structure

Figure 6 presented the microstructure of CVTP detected by SEM under different B_2O_3 addition amounts. Results of XRD analysis of CVTP with B_2O_3 addition suggested that, the B_2O_3 mainly existed in the forms of $TiB_{0.024}O_2$ and Fe_3BO_5 on the phase composition of CVTP during oxidation induration. Meanwhile, no peaks of B_2O_3 could be identified at the B_2O_3 addition amount of 2−6 wt.%, which could be attributed to the reaction of B_2O_3 with Fe_3O_4 and Fe_2TiO_5. Hence, the microstructure of CVTP under different B_2O_3 addition amounts should be further investigated to examine the effect of B-bearing phases on the mineragraphy and structure of CVTP. Figure 6(a) exhibited the microstructure of CVTP in the absence of B_2O_3 addition, and the inter-grain intervals were distinct with little closed pores, which corresponded to the low porosity; besides, the grain size distribution was relatively uniform. Meanwhile, the gangue mineral also existed among the individual hematite grains. Besides, the silicate phases mainly acted as the binder phases among the hematite grain boundaries, which could form a continuous structure and decrease the cracks, giving rise to the relatively high CS of CVTP in the absence of B_2O_3 addition. At the B_2O_3 addition of 2 wt.%, many small and square-shaped

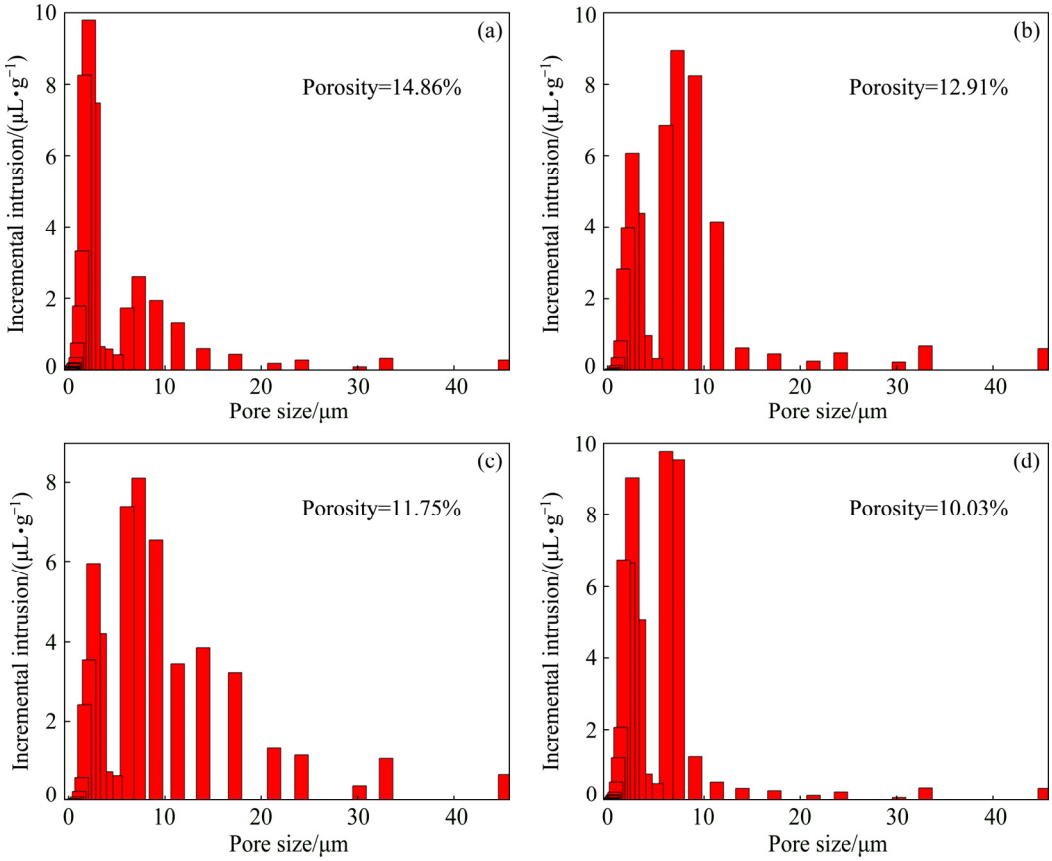

Fig. 5 Porosity and pore size distribution of CVTP with different B_2O_3 addition amounts: (a) 0 wt.%; (b) 2 wt.%; (c) 4 wt.%; (d) 6 wt.%

grains, including the hematite and B-bearing phases, were connected by the silicate phases, which had existed among the intervals of large hematite grains, as shown in Fig. 6(b). Although the small particles had disadvantage to the strength between adjacent hematite grains, the silicate phases that served as the bonding phase would improve the strength of structure. On the other hand, the irregular huge and small hematite grains could be observed in Fig. 6(b). Analysis of points A and B suggested that, the B-bearing spinel and silicate compounds distributed along the grain boundaries and pores. Obviously, the hematite grains gathered gradually, which would reduce the porous structure. Hence, the CS of CVTP would be increased while the porosity of CVTP would be increased at the B_2O_3 addition of 2 wt.%, indicating the positive effect on the bonding of hematite grains and silicate phases.

Furthermore, the sizes of hematite grains would be slightly increased at the B_2O_3 addition up to 4 wt.%. Figure 6(c) displayed the hematite grains, mixed silicate and small grain phases. As could be observed, the small grains would gather together with the cohesive silicate phases. Therefore, the CS of CVTP would be decreased in the presence of 4 wt.% B_2O_3 addition. Besides, when the B_2O_3 addition was increased to 6 wt.%, the microstructure of CVTP became more uniform and compact. The hematite grains became greater, and the small grains would mix with silicate phases and distributed on huge hematite boundaries and pores. Moreover, the quantity of pores would be decreased, while the pore size would be increased with 6 wt.% B_2O_3 addition. Figure 7 presented the EDS analysis results of CVTP with 6 wt.% B_2O_3 addition. Clearly, for points A, B and C, the contents of B_2O_3 were 4.12, 6.51 and 8.56 wt.%, respectively. The EDS result of point A demonstrated that, the light gray area was indicative of the compound of hematite, B-bearing, Mg-bearing and Ti-bearing spinels; by contrast, the EDS of point B suggested that the gray area represented the compound of fayalite and B-bearing phase, which distributed on the pore edge. Analysis of point C indicated that, the dark gray area was made of B-bearing and silicate phases. Typically, B_2O_3 addition would give rise to the compact and dense structure, alone with huge hematite grains, B-bearing spinels, and silicate phases. Moreover, the B-doped Ti-bearing spinel was combined with hematite, as shown in point A of Fig. 7(a). Notably, the huge hematite and concentrated silicate phases were advantageous to improving CS, but these structures would decrease the porosity of CVTP.

Figure 8 presents the elemental distributions of Fe, B, Ti, V, and Cr in CVTP with 6 wt.% B_2O_3 addition.

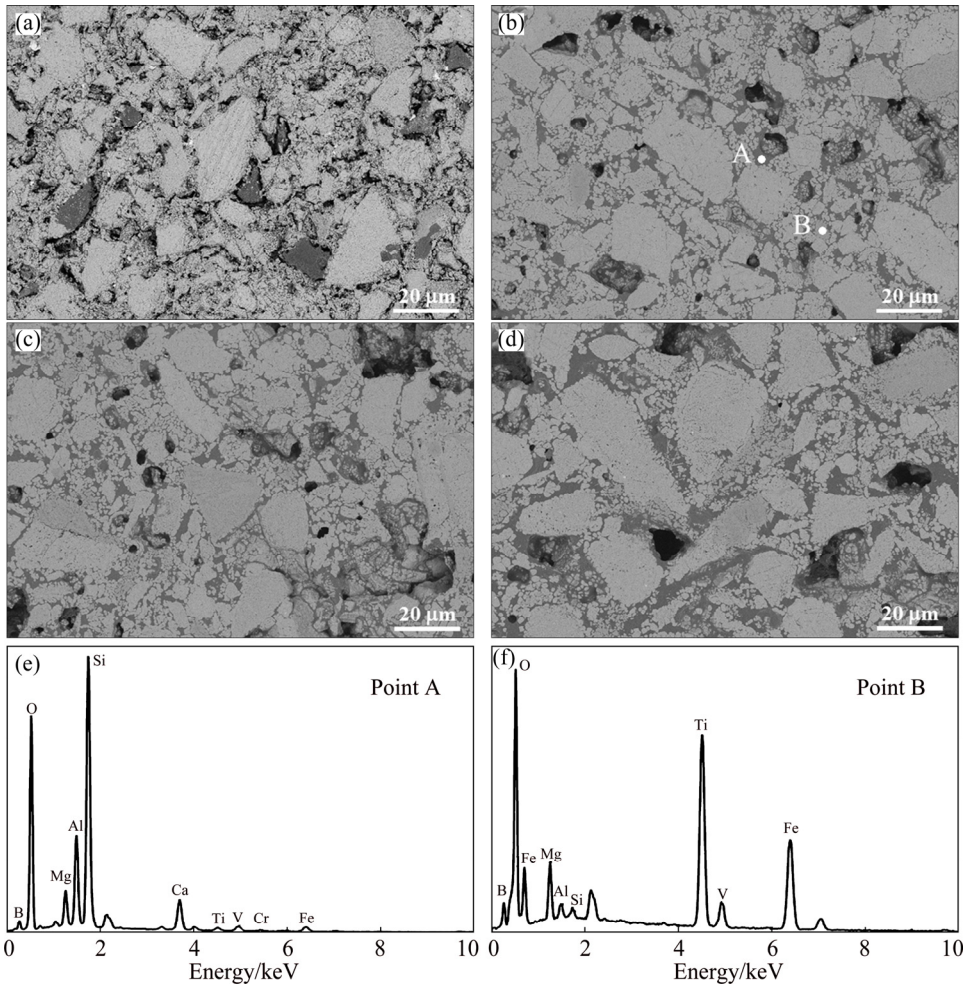

Fig. 6 SEM images (a−d) and EDS analysis results (e, f) of CVTP with different B_2O_3 addition amounts: (a) 0 wt.%; (b) 2 wt.%; (c) 4 wt.%; (d) 6 wt.%; (e) Point A; (f) Point B

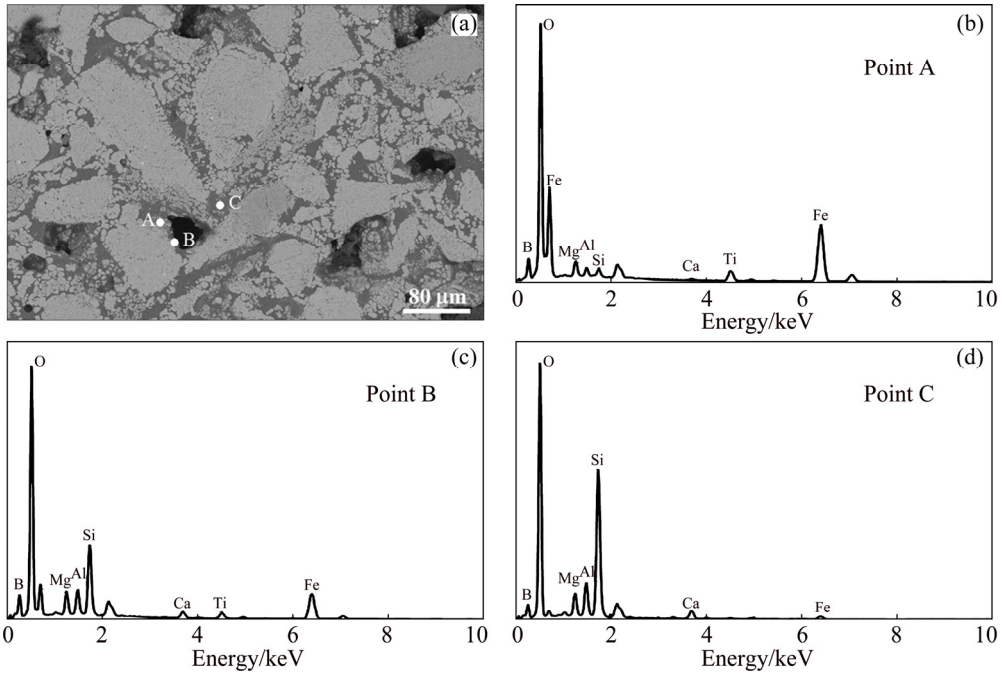

Fig. 7 SEM image (a) and EDS analysis results (b−d) of CVTP with 6 wt.% B_2O_3 addition

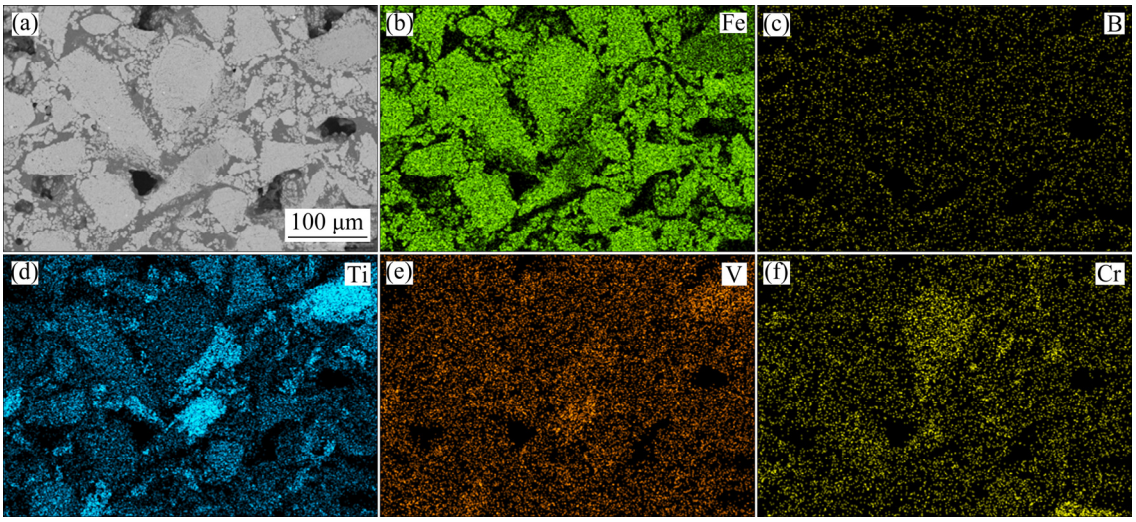

Fig. 8 X-ray element mapping of CVTP with 6 wt.% B_2O_3 addition

It could be seen from Fig. 8 that, the B mainly existed in the intervals of hematite grains; at the same time, a small portion of B would coexist with Ti and Fe elements to generate the $TiB_{0.024}O_2$ and Fe_3BO_5 phases, respectively. On the other hand, Cr and V mainly existed in iron oxides, among which, a little portion of V would combine with Ti to form spinels. Besides, a portion of Ti would bind with Fe to form Fe_2TiO_5. Taken together, the above analyses indicated that, B_2O_3 addition would improve the microstructure and recrystallization of hematite grains, which could further increase the bonding phase of CVTP during oxidation induration, finally resulting in the increased CS of CVTP.

According to the above results, the B_2O_3 addition had a stimulative effect on the recrystallization of hematite grains, grain size, and bonding phases at the intervals of mineral grains, but the micropore structure would be reduced with the increase in B_2O_3 addition. In addition, the hematite grains would be interconnected with micropores, which distributed in a relatively uniform way in the absence of B_2O_3 addition. Moreover, the hematite grains could be fully recrystallized and connected, along with larger micropores and more bonding phases at the intervals of grains, which could enhance the CS of CVTP. Nevertheless, the size of hematite grain would be increased and became uniform. Additionally, B_2O_3 could also react with elements Ti and Fe to generate $TiB_{0.024}O_2$ and Fe_3BO_5, respectively, on the grain boundaries. Therefore, B_2O_3 addition was beneficial to the oxidation induration of CVTP, which could also improve the CS of CVTP.

3.2 Swelling behavior of CVTP

3.2.1 Phase composition

Figure 9 displayed the XRD patterns of CVTP reduced for 60 min under different B_2O_3 addition amounts. As could be observed, the XRD pattern displayed the gradual change in the peak with B_2O_3 addition, indicating that the B_2O_3 addition would partially affect the phase composition of the reduced CVTP. The primary phases of the reduced CVTP in the absence of B_2O_3 addition were Fe, FeO and Fe_2TiO_4. Besides, the peak intensities of the new phases $TiB_{0.024}O_2$ and Fe_3BO_5 would be strengthened with the increase in B_2O_3 addition, and the B-bearing phase might also affect the physical characteristics of the reduced CVTP. LIU et al [21] had investigated that Fe_2TiO_4 was one of the reduced products of iron titanium with H_2. Meanwhile, the peak intensity of Fe would be slightly reduced, whereas the peak intensities of Fe_2TiO_4, $TiB_{0.024}O_2$ and Fe_3BO_5 would be increased with B_2O_3 addition. However, B_2O_3 was not detected in the reduced CVTP, which could be ascribed to the difficult reduction of $TiB_{0.024}O_2$ and Fe_3BO_5.

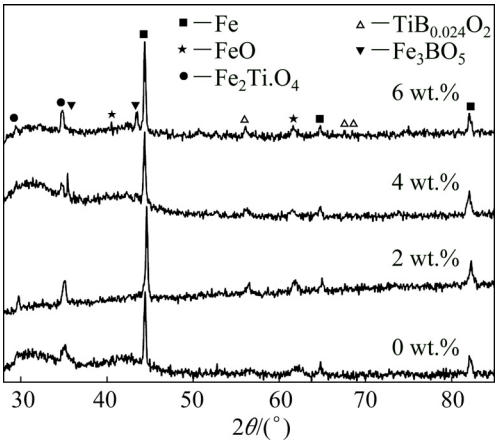

Fig. 9 XRD patterns of reduced CVTP with different B_2O_3 addition amounts

The main possible reactions during the reduction of CVTP with simulated COG could be classified as the

reduction of Fe_2O_3, Fe_2TiO_5, Fe−B and Ti−B compounds, as well as the side reactions of the products. The possible chemical reactions are simply presented in Fig. 10. Equations (10)−(13) and Eqs. (16)−(19) were the possible reduction reactions of hematite by CO and H_2, while Eqs. (14) and (20) were the possible reduction reactions of Fe_2TiO_5 with CO and H_2, respectively. Figure 10 has displayed the relation between ΔG^{Θ} and T for possible reduction reactions of CVTP. According to the calculated results, the ΔG^{Θ} lines of Eqs. (15) and (21) were above the zero line, suggesting that the boron oxide could be hardly reduced due to the thermodynamic stability. Moreover, the ΔG^{Θ} lines of Eqs. (14) and (20) were below the zero line, revealing that the Fe_2TiO_5 could be easily reduced by CO and H_2 to generate Fe_2TiO_4.

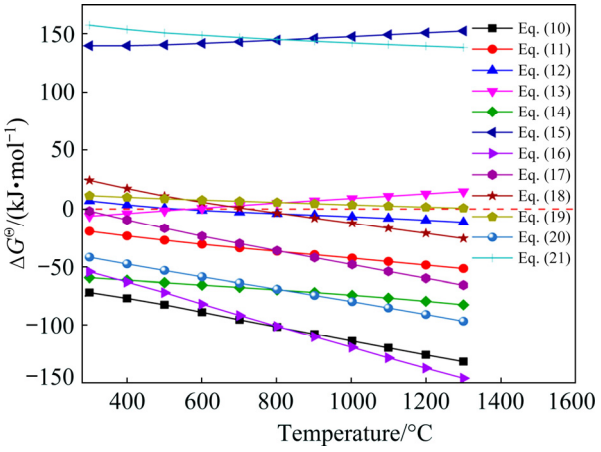

Equation	Reaction
(10)	$3Fe_2O_3+CO=2Fe_3O_4+CO_2$
(11)	$Fe_2O_3+CO=2FeO+CO_2$
(12)	$Fe_3O_4+CO=3FeO+CO_2$
(13)	$FeO+CO=Fe+CO_2$
(14)	$Fe_2TiO_5+CO=Fe_2TiO_4+CO_2$
(15)	$1/3B_2O_3+CO=2/3B+CO_2$
(16)	$3Fe_2O_3+H_2=2Fe_3O_4+H_2O$
(17)	$Fe_2O_3+H_2=2FeO+H_2O$
(18)	$Fe_3O_4+H_2=3FeO+H_2O$
(19)	$FeO+H_2=Fe+H_2O$
(20)	$Fe_2TiO_5+H_2=Fe_2TiO_4+H_2O$
(21)	$1/3B_2O_3+H_2=2/3B+H_2O$

Fig. 10 Relation between ΔG^{Θ} and T for possible reduction reactions of CVTP

3.2.2 Effect of B_2O_3 addition on RSI

Figure 11 presented the effect of B_2O_3 addition on the RSI and CS of the reduced CVTP with simulated COG. Obviously, the RSI was decreased from 5.87% to 3.81% while the CS was increased from 901 to 956.2 N, with the increase in B_2O_3 addition amounts. SHARMA et al [22] had examined the effect of oxidation induration on the reduction swelling behavior of pellets, and discovered that the increasing CS while decreasing porosity of pellets would result in the decreasing RSI. As a result, the CS and porosity of pellets would affect their RSI. The low reduction swelling pellet could be mainly ascribed to the presence of slag bonds, which could not mechanically push the adjacent grains and would lead to the decrease in volume [23]. Moreover, the generation of iron whiskers during reduction would also induce more stresses onto the pellets, rendering higher reduction swelling and less CS of CVTP. Therefore, the decreased reduction swelling behavior of CVTP would be affected by the as-generated iron whiskers under the impact of B_2O_3 addition. In the meantime, the initial high porosity of pellets indicated fast reduction and less reduction swelling [24]. Previously, the reduction swelling of pellets usually reached a maximum value at about 900 °C by CO within the temperature range of 800−1100 °C, which was related to the formation of a mass of whiskers at about 900 °C [25]. YI et al [26] suggested that H_2 addition into the reduction atmosphere would reduce the swelling and expansion characteristics of pellets, which would lead to a higher CS of pellets, since the pellets had rapidly passed the Wüstite stage and the pellets bonding had been remarkably improved.

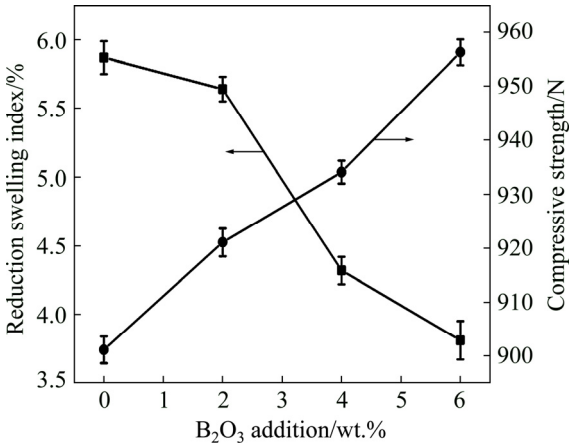

Fig. 11 Effect of B_2O_3 additions on RSI and CS of reduced CVTP

3.2.3 Microscopic structure

To reveal the underlying mechanisms of reduction swelling behavior and CS of the reduced CVTP, the microstructures of the reduced CVTP were detected under different B_2O_3 addition amounts. The results were shown in Fig. 12. It could be indicated that, B_2O_3 addition would prominently affect the microstructures of the reduced CVTP. As could be seen from Fig. 12(a), the microstructure of the reduced CVTP was reticular and

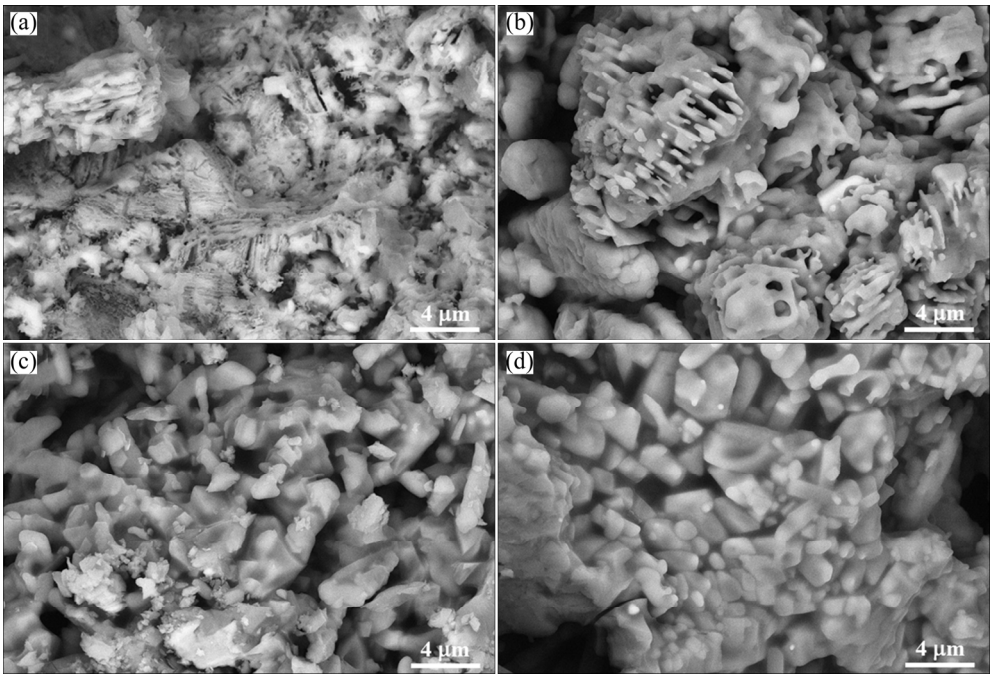

Fig. 12 SEM images of reduced CVTP with different B_2O_3 addition amounts: (a) 0 wt.%; (b) 2 wt.%; (c) 4 wt.%; (d) 6 wt.%

filiform; meanwhile, the metallic iron whiskers existed in the reticular structure. Consequently, the generation of metallic iron whiskers would give rise to the reticular structure as well as reduction swelling of CVTP. It could be seen from Fig. 12(b) that, more round dots and shorter metallic iron whiskers had been generated on the surfaces of lamellar grains at the B_2O_3 addition of 2 wt.%. Besides, the lamellar grains of CVTP with 2 wt.% B_2O_3 addition became denser than those of CVTP without B_2O_3 addition. Typically, the metallic iron whiskers and round dots of the metallic iron would accumulate together at the B_2O_3 addition of 4 wt.%, while the lamellar crystals would apparently disappear, as presented in Fig. 12(c). Besides, individual grains would be generated and aggregate on the CVTP surface. Moreover, the RSI of CVTP would be further decreased at the B_2O_3 addition up to 6 wt.%, as could be seen in Fig. 11. From the microstructure of Fig. 12(d), the individual grains would grow gradually and would be bonded by silicate phases, and such structure would improve the intensity of CVTP. In addition, the pores and intervals would be reduced with the bonding property of silicate phases when the B_2O_3 addition was elevated to 6 wt.%. Under these conditions, the generation of metallic iron whiskers was restrained and the shape of metallic iron had changed from round dots to individual particles with the increase in B_2O_3 addition. As could be determined from the microstructure of the reduced CVTP, a large number of metallic iron whiskers could be detected in the absence of B_2O_3 addition. However, nucleation points of metallic iron particles would be generated in the microstructure of the reduced CVTP when the B_2O_3 addition was higher than 2 wt.%; meanwhile, the aggregation and diffusion of metallic iron would be enhanced gradually with the increase in B_2O_3 addition during the reduction process with COG injection. On the other hand, the quantity of pores would be reduced with the aggregation of mineral grains, thereby leading to weakened swelling behavior of CVTP with the increase in B_2O_3 addition.

According to the above analyses, many round dots of metallic iron would be formed on the surface of lamellar crystals; in addition, the thick interval of lamellar crystals would also be formed with B_2O_3 addition. Under such condition, the CS of the reduced CVTP would be increased while the RSI would be reduced with the subdued swelling behaviors. In the presence of high B_2O_3 addition, the aggregation and diffusion of metallic iron would enhance the CS of the reduced CVTP; on this account, B_2O_3 addition would restrain the reduction swelling of CVTP and facilitate the increase in CS of CVTP. WANG and SOHN [25] investigated the swelling behavior of iron ore during the reduction process, and found that the metal iron whiskers would induce swelling as crucial factor. Moreover, B_2O_3 addition would lower the formation of metal iron whiskers and weaken the swelling behavior.

4 Conclusions

(1) The primary phases of CVTP with B_2O_3 addition were Fe_2O_3, Fe_2TiO_5, $TiB_{0.024}O_2$ and Fe_3BO_5. The

compressive strength of CVTP was increased from 2448 to 3819.2 N; meanwhile, the porosity was decreased from 14.86% to 10.03% with the increase in B_2O_3 additions.

(2) The micron pore size distribution of CVTP mainly distributed between 0 to 5 μm at the B_2O_3 addition lower than 2 wt.%, and the proportion of micron pore size distribution of CVTP was notably decreased, while the pore size distribution of CVTP between 5 and 30 μm was increased at the B_2O_3 addition higher than 4 wt.%.

(3) The primary phases of the reduced CVTP with B_2O_3 addition were Fe, FeO, Fe_2TiO_4, $TiB_{0.024}O_2$ and Fe_3BO_5.

(4) The reduction swelling index was reduced from 5.87% to 3.81%, whereas the compressive strength was elevated from 901 to 956.2 N with the increase in B_2O_3 addition.

References

[1] TAKANO C, ZAMBRANO A P, NOGUEIRA A E A, MOURAO M B, IGUCHI Y. Chromites reduction reaction mechanisms in carbon–chromites composite agglomerates at 1773 K [J]. ISIJ International, 2007, 47(11): 1585−1589.

[2] LU Chang-yuan, ZOU Xing-li, LU Xiong-gang, XIE Xue-liang, ZHENG Kai, XIAO Wei, CHENG Hong-wei, LI Guang-shi. Reductive kinetics of Panzhihua ilmenite with hydrogen [J]. Transactions of Nonferrous Metals Society of China, 2016, 26(12): 3266−3273.

[3] CHENG Gong-jin, XUE Xiang-xin, GAO Zi-xian, JIANG Tao, YANG He, DUAN Pei-ning. Effect of Cr_2O_3 on the reduction and smelting mechanism of high-chromium vanadium−titanium magnetite pellets [J]. ISIJ International, 2016, 56(11): 1938−1947.

[4] JENA B C, DRESLER W, REILLY I G. Extraction of titanium, vanadium and iron from titanomagnetite deposits at pipestone lake [J]. Manitoba, Canada, Minerals Engineering, 1995, 8(1): 159−168.

[5] CHENG Gong-jin, GAO Zi-xian, YANG He, XUE Xiang-xin. Effect of calcium oxide on the crushing strength, reduction, and smelting performance of high-chromium vanadium-titanium magnetite pellets [J]. Metals, 2017, 7(6): 181−194.

[6] CHENG Gong-jin, XUE Xiang-xin, JIANG Tao, DUAN Pei-ning. Effect of TiO_2 on the crushing strength and smelting mechanism of high-chromium vanadium−titanium magnetite pellets [J]. Metallurgical and Materials Transactions B, 2016, 47(3): 1713−1726.

[7] MAHESWARAN V S, KUMAR B S, EDUARD H, ANGELA V, SIGURD B, FRANSISCO C, LARS N. Enhanced densification of PM steels by liquid phase sintering with boron-containing master alloy [J]. Metallurgical and Materials Transactions B, 2018, 49(1): 255−263.

[8] BIAN Yu-yang, GUO Shu-qiang, JIANG Lan, LIU Jie, TANG Kai, DING Wei-zhong. Recovery of rare earth elements from NdFeB magnet by VIM-HMS method [J]. ACS Sustainable Chemistry & Engineering, 2016, 4(3): 810−818.

[9] WANG Guang, XUE Qing-guo, WANG Jing-song. Effect of Na_2CO_3 on reduction and melting separation of ludwigite/coal composite pellet and property of boron-rich slag [J]. Transactions of Nonferrous Metals Society of China, 2016, 26(1): 282−293.

[10] FU Xiao-jiao, CHU Man-sheng, GAO Li-hua, LIU Zheng-gen. Stepwise recovery of magnesium from low-grade ludwigite ore based on innovative and clean technological route [J]. Transactions of Nonferrous Metals Society of China, 2018, 28(11): 2383−2394.

[11] WANG Bin, LI He-jun, ZHANG Yu-lei, WANG Qian. Preparation and oxidation resistance of B_2O_3-coated boron-modified carbon foams [J]. Transactions of Nonferrous Metals Society of China, 2013, 23(7): 2123−2128.

[12] GAO Yan-hong, BIAN Ling-tao, LIANG Zhong-yu. Influence of B_2O_3 and TiO_2 on viscosity of titanium-bearing blast furnace slag [J]. Steel Research International, 2015, 86(4): 386−390.

[13] REN Shan, ZHANG Jian-liang, WU Liu-shun, LIU Wei-jian, BAI Ya-nan, XING Xiang-dong, SU Bu-xin, KONG De-wen. Influence of B_2O_3 on viscosity of high ti-bearing blast furnace slag [J]. ISIJ International, 2012, 52(6): 984−991.

[14] SUN Yong-qi, LIAO Jun-lin, ZHENG Kai, WANG Xi-dong, ZHANG Zuo-tai. Effect of B_2O_3 on the structure and viscous behavior of Ti-bearing blast furnace slags [J]. JOM, 2014, 66(10): 2168−2175.

[15] XU Ren-ze, ZHANG Jian-liang, WANG Zhi-yu, JIAO Ke-xing. Influence of Cr_2O_3 and B_2O_3 on viscosity and structure of high alumina slag [J]. Steel Research International, 2017, 88(4): 1600241.

[16] SONMEZOGLU S, ERDOĞAN B, ASKEROĞLU I. Investigation of optical, structural and morphological properties of nanostructured boron doped TiO_2 thin films [J]. Bulletin of Materials Science, 2014, 36(7): 1239−1245.

[17] PTAČINOVá J, DRIENOVSKY M, PALCUT M, ČIČKA R, KUSÝ M, HUDÁKOVÁ M. Oxidation stability of boride coatings [J]. Kovove Materialy, 2015, 53(3): 1−12.

[18] ZHANG Yi-min. Pellet production technology [M]. Beijing: Metallurgical Industry Press, 2005. (in Chinese)

[19] OROWAN E. Fracture and strength of solids [J]. Reports on Progress in Physics, 1949, 12(1): 185−232.

[20] SPRIGGS R M. Expression for effect of porosity on elastic modulus of polycrystalline refractory materials, particularly aluminum oxide [J]. Journal of the American Ceramic Society, 1961, 44(12): 628−629.

[21] LIU Yu-cheng, NACHIMUTHU S, CHUANG Yu-cheng, KU Y, JIANG J C. Reduction mechanism of iron titanium based oxygen carriers with H_2 for chemical looping applications–A combined experimental and theoretical study [J]. RSC Advances, 2016, 6(108): 106340−106346.

[22] SHARMA T, GUPTA R C, PRAKASH B. Swelling of iron ore pellets by statistical design of experiment [J]. ISIJ International, 1992, 32(12): 1268−1275.

[23] SEATON C E, FOSTER J S, VELASCO J. Structural changes occurring during reduction of hematite and magnetite pellets containing coal char [J]. Transactions of the Iron and Steel Institute of Japan, 1983, 23(6): 497−503.

[24] KANG T, GUPTA S, SAHAJWALLA V. Characterizing swelling behaviour of iron oxides during solid state reduction for corex application and their implications on fines generation [J]. ISIJ International, 2007, 47(11): 1590−1598.

[25] WANG Hai-tao, SOHN H Y. Effects of firing and reduction conditions on swelling and iron whisker formation during the reduction of iron oxide compact [J]. ISIJ International, 2011, 51(6): 906−912.

[26] YI Ling-yun, HUANG Zhu-cheng, JIANG Tao, WANG Li-na, QI Tao. Swelling behavior of iron ore pellet reduced by H_2–CO mixtures [J]. Powder Technology, 2015, 269: 290−295.

B_2O_3对含铬型钒钛磁铁矿球团氧化固结及在喷吹焦炉煤气时还原膨胀行为的影响

汤卫东[1]，杨松陶[2]，薛向欣[1]

1. 东北大学 冶金学院，沈阳 110819；
2. 辽宁科技大学 材料与冶金学院，鞍山 114051

摘　要：研究 B_2O_3 对含铬型钒钛磁铁矿球团氧化固结和还原膨胀行为的影响。在模拟喷吹焦炉煤气的条件下，研究球团还原膨胀指数和抗压强度。结果表明，随着 B_2O_3 含量的提高，球团的抗压强度从 2448 N 增至 3819.2 N，而孔隙率从 14.86%降至 10.03%。添加的 B_2O_3 主要以 $TiB_{0.024}O_2$ 和 Fe_3BO_5 的形式存在于氧化球团和还原球团中。随着 B_2O_3 含量的提高，还原球团的抗压强度从 901 N 提高至 956.2 N，还原膨胀指数从 5.87%降低至 3.81%。B_2O_3 能促进金属铁的聚集和扩散，抑制铁晶须的形成，并降低还原膨胀行为。

关键词：B_2O_3；氧化固结；还原膨胀指数；焦炉煤气；含铬型钒钛磁铁矿球团

(Edited by Bing YANG)